



## 1 A Predictive Algorithm For Wetlands In Deep Time Paleoclimate Models

2 David J. Wilton<sup>1</sup>, Marcus Badger<sup>2,3,4</sup>, Euripides P. Kantzas<sup>1</sup>, Richard D. Pancost<sup>3</sup>, Paul J.  
3 Valdes<sup>4</sup>, David J. Beerling<sup>1</sup>

4

5 <sup>1</sup>Dept. Animal and Plant Sciences, The University of Sheffield, Sheffield, S10 2TN, UK

6 <sup>2</sup>School of Environment, Earth and Ecosystem Sciences, The Open University, Milton  
7 Keynes, MK7 6AA

8 <sup>3</sup>Organic Geochemistry Unit, The Cabot Institute, School of Chemistry, School of Earth  
9 Sciences, The University of Bristol, Bristol, BS8 1TH, UK

10 <sup>4</sup>Bristol Research Initiative for the Dynamic Global Environment (BRIDGE), The Cabot  
11 Institute, School of Geographical Sciences, The University of Bristol, BS8 1TH, UK

12 *Correspondence to:* David J. Wilton ([d.j.wilton@shef.ac.uk](mailto:d.j.wilton@shef.ac.uk))

13

14 **Abstract.** Methane is a powerful greenhouse gas produced in wetland environments via  
15 microbial action in anaerobic conditions. If the location and extent of wetlands are unknown,  
16 such as for the Earth many millions of years in the past, a model of wetland fraction is  
17 required in order to calculate methane emissions and thus help reduce uncertainty in the  
18 understanding of past warm greenhouse climates. Here we present an algorithm for predicting  
19 inundated wetland fraction for use in calculating wetland methane emission fluxes in deep  
20 time paleoclimate simulations. The algorithm determines, for each grid cell in a given  
21 paleoclimate simulation, the wetland fraction predicted by a nearest neighbours search of  
22 modern day data in a space described by a set of environmental, climate and vegetation  
23 variables. To explore this approach, we first test it for a modern day climate with variables  
24 obtained from observations and then for an Eocene climate with variables derived from a  
25 fully coupled global climate model (HadCM3BL-M2.2). Two independent dynamic  
26 vegetation models were used to provide two sets of equivalent vegetation variables which  
27 yielded two different wetland predictions. As a first test the method, using both vegetation  
28 models, satisfactorily reproduces modern data wetland fraction at a coarse grid resolution,  
29 similar to those used in paleoclimate simulations. We then applied the method to an early  
30 Eocene climate, testing its outputs against the locations of Eocene coal deposits. We predict  
31 global mean monthly wetland fraction area for the early Eocene of  $8$  to  $10 \times 10^6$  km<sup>2</sup> with  
32 corresponding total annual methane flux of  $656$  to  $909$  Tg CH<sub>4</sub> year<sup>-1</sup>, depending on which of  
33 two different dynamic global vegetation models are used to model wetland fraction and  
34 methane emission rates. Both values are significantly higher than estimates for the modern-  
35 day of  $4 \times 10^6$  km<sup>2</sup> and around  $190$  Tg CH<sub>4</sub> year<sup>-1</sup> (Poulter et. al. 2017, Melton et. al., 2013).

36

## 37 1 Introduction

38 Methane (CH<sub>4</sub>) is a powerful greenhouse gas. As well as absorbing infrared radiation from  
39 the Earth's surface it also contributes to additional indirect warming through its



40 photochemistry and oxidation to CO<sub>2</sub> in the atmosphere (IPCC 2013). Therefore, Earth  
41 system models used to reconstruct ancient climate or develop future climate scenarios must  
42 either assume atmospheric methane concentrations as a boundary condition and/or  
43 incorporate dynamic methane fluxes from natural sources (Beerling et al. 2011). The main  
44 natural source of methane is wetland environments via microbial action in anaerobic  
45 conditions (Whiticar, 1999), but methane fluxes from wetlands are also modulated by  
46 climatic factors such as temperature (Westermann, 1992). Therefore, in order to model fluxes  
47 of methane to the atmosphere both the extent and locations of wetlands need to be known.  
48 For modern day, recent past and near future scenarios, maps of observed wetland extent  
49 (Prigent et al. 2007, Papa et al. 2010, Schroeder et al., 2015, Poulter et al, 2017) can be used  
50 or wetland extent can be calculated at a sub-grid level from fine resolution topographical data  
51 (as in the TOPMODEL approach of Beven and Kirkby (1979), Lu and Zhuang (2012),  
52 Stocker et al. (2014), Lu et al. (2016)), as wetlands only form where the ground is relatively  
53 flat.

54 For the study of deep time paleoclimates (many millions of years in the past) there are no  
55 direct observations of wetland extent, and the topography is only known on relatively coarse  
56 resolutions of around 0.5 ° at best. Therefore, any model calculation of wetland extent must  
57 either rely on using approximate knowledge of the topography or not rely on the topography  
58 at all. Previous studies (Beerling et al., 2011, Valdes et al., 2005) classified grid cells as either  
59 producing or not producing methane, based on either: i) a month being within a defined melt  
60 season, for grid cells where mean monthly temperature drops below 0 °C at some point in the  
61 year; or ii) precipitation being greater than evapotranspiration. They then scaled emissions by  
62 empirically derived functions of the variance or standard deviation of orography, at the best  
63 resolution available. The scaling effectively reduces methane emission rates in grid cells  
64 where elevation varies significantly and are therefore unlikely to have substantial wetlands  
65 within them, but relies on what may be quite coarse resolution topography not able to resolve  
66 sub-grid scale variations.

67 In this work we develop a nearest neighbour-based algorithm to predict the fraction of a  
68 specified area that is wetland (FW). We base this on modern day reference data set of FW  
69 and corresponding environmental variables, empirically associating the FW observations with  
70 corresponding observed climate data and vegetation data calculated using one of two  
71 dynamic global vegetation models (DGVMs). We demonstrate its application by predicting  
72 FW and CH<sub>4</sub> fluxes for an early Eocene (52 Ma) model climate, an interval of greenhouse  
73 warming (Zachos et al., 2008) when sedimentary records indicate the existence of large areas  
74 of wetlands (Sloan et al., 1992, Beerling et al., 2009). For the Eocene, the same climate  
75 variables are obtained from a fully coupled global climate model and vegetation variables are  
76 derived from the same DGVMs. We then predict FW for the Eocene by analysis and  
77 comparison to the modern-day reference data. We note that different reference sets,  
78 vegetation models or climate models will likely yield different results and these should be  
79 explored in future work, but our aim here is to demonstrate this approach and its potential  
80 rather than to produce a model-model intercomparison.

81 Firstly, we describe modern day wetland data at 0.5° spatial resolution and a monthly time  
82 step for a mean modern day year, along with climate and vegetation data which we later use  
83 as a reference data set. We then describe two test data sets at lower spatial resolution,



equivalent to that used in paleoclimate models, again for a single year. The first of these is for the modern day and derived by interpolation of the reference data and the second is derived from a paleoclimate model of the early Eocene. We briefly describe unsuccessful attempts to model FW before moving on to the Nearest Neighbours method we found to be successful. We also describe the model used to calculate wetland methane emissions. We then discuss the model results for the modern day test data set and then Early Eocene climate. For the modern day test data set the nearest neighbour method should yield strong agreement, since it is simply a downscaled version of the reference data; these results, therefore, serve to demonstrate whether or not a generalised form of the method can be successfully applied to prediction of FW for a climate very different to the modern day. We then apply this method to prediction of FW for the Eocene, and show that we can tune it by using the locations of coal deposits as wetland proxies.

96

## 97 **2 Data and Methods**

### 98 **2.1 Modern day reference data**

We use a modern-day reference data set of observed FW with corresponding environmental data to develop an algorithm for the prediction of FW in the past, i.e. we assume that there exists a relationship between FW and the environmental variables compiled in the reference data and then apply that relationship to predicting FW in the past. We use the recently developed SWAMPS-GLWD (Poulter et al., 2017), which improves on the Surface Water Microwave Product Series (SWAMPS) (Schroeder et al., 2015) by adding Global Lakes and Wetlands Database (GLWD) (Lehner and Doll 2004) data, correcting the SWAMPS dataset in regions where this satellite derived dataset fails to detect water beneath closed canopies. We calculated the average monthly FW at each  $0.5^\circ \times 0.5^\circ$  grid cell for the years 2000 to 2012 on a monthly time step to give a modern-day FW ( $FW_{obs}$ ; annual max shown in Figure 1). Corresponding climate data on the same spatial and temporal resolution were obtained from CRU-NCEP v4.0 (Wei et al. 2014) and averaged to give monthly values for a mean modern-day year over the same time interval. The climate data for this mean year were then used to drive two DGVMs: the Sheffield Dynamic Global Vegetation Model (SDGVM) (Woodward et al., 1995; Beerling and Woodward, 2001) and the Lund-Postdam-Jenna model (LPJ) (Wania et al., 2009) to produce corresponding vegetation data. The combination of these yielded a reference data set of FW, climate (temperature and precipitation) and vegetation (leaf area index, net primary productivity, transpiration, evapotranspiration, soil water content and surface runoff) variables (either SDGVM or LPJ) for a set of  $0.5^\circ \times 0.5^\circ$  spatial and monthly temporal resolution sites for a single modern-day average year. To ensure that wetlands in areas dominated by agriculture or where one of our vegetation models, SDGVM, predicts bare land, did not bias our FW predictions, such grid cells were removed from the reference data. For the latter, this was done simply by removing those grid cells that SDGVM predicted to be bare land. For the former, we removed those that were 50 % or more, by cover, classed as cultivated and managed or mosaic cropland (Global Land Cover 2000 database, 2003).

Many of the methods that can be used to analyse the reference data and predict FW require that the data are scaled, so that each variable covers a similar range of values. Therefore, we



127 scaled the values of each environmental variable,  $X$ , using their mean,  $\mu_x$ , and standard  
128 deviation,  $\sigma_x$ , i.e. for a given grid cell,  $J$ , each variable was scaled as:

$$129 \quad X'(J) = \frac{X(J) - \mu_x}{\sigma_x} \quad (1)$$

130 This scales all variables such that they have mean of 0 and standard deviation 1.

## 131 2.2 Test data sets

132 A modern-day test set was made by interpolating the reference climate data to  $2.5^\circ \times 3.75^\circ$ ,  
133 the spatial resolution often used for paleoclimate models. The DGVMs simulations were  
134 conducted on this interpolated data to yield the vegetation outputs. All climate and vegetation  
135 variables were scaled in the same way as the reference data, using the means and standard  
136 deviations of the reference data. The palaeoclimatic assessment of our model was performed  
137 using an early Eocene three dimensional fully dynamic coupled ocean-atmosphere global  
138 climate model HadCM3BL-M2.2 (Valdes et al., 2017), on a  $2.5^\circ$  latitude by  $3.75^\circ$  longitude  
139 grid and at a monthly time step for a single year. To simulate the early Eocene a Ypresian  
140 paleogeography and high  $\text{CO}_2$  (4x modern; 1120 ppm; Agnostous et al., 2016) was used.  
141 SDGVM and LPJ were both run with these model-simulated climate data to produce the  
142 vegetation variables required, as was done for the reference data set, whereas temperature and  
143 precipitation were derived directly from the climate model. All variables were again scaled  
144 using the means and standard deviations of the reference data. Therefore, for each climate,  
145 modern day and early Eocene, we have two test data sets for a mean year on a monthly time  
146 step, at  $2.5^\circ \times 3.75^\circ$  spatial resolution, both with the same climate data, one with SDGVM  
147 vegetation data and one with LPJ vegetation data. Predictions for each test data set were  
148 made with the corresponding vegetation model's reference data set.

149

## 150 2.3 Initial unsuccessful models of wetland fraction

151 Before discussing the model we employed to predict paleoclimate FW, it is useful to describe  
152 briefly other strategies that we attempted but that did not yield robust predictions when  
153 evaluated against modern-day data. The first of these was to examine FW vs individual  
154 environmental variables graphically from the reference data, to ascertain if we could define  
155 ranges for those variables that corresponded to predominantly low or high FW; this is similar  
156 to the approach of Shindell et al. (2004), who proposed threshold values of standard deviation  
157 of topography, ground temperature, ground wetness and downward shortwave flux for  
158 wetland development. However, this proved unsuccessful, revealing only the rather obvious  
159 relationship that wetlands do not usually occur when mean monthly temperature is below  $0^\circ\text{C}$ .  
160 Although we expected to identify relationships for FW with other environmental  
161 variables (i.e. ground wetness), none were found. This is due to the combined effects of  
162 wetland occurrence being the function of multiple factors and the fact that most grid cells  
163 have  $\text{FW} \approx 0$  for all months of the year and the number with significantly non-zero FW is  
164 quite small. Therefore, environmental variables associated with high values of FW also tend  
165 to be associated with  $\text{FW} \approx 0$ . Poor correlation of FW with environmental variables is also  
166 due to the important control exerted by the topography; regardless of climate, wetlands  
167 cannot form in landscapes where excess water flows away rather than remaining in situ.



Collectively, these factors caused significant overlap in the range of environmental variables associated with both low and high FW.

Another approach was a multiple linear regression using the reference data in order to derive an equation for FW in terms of linear functions of multiple environmental variables. However, this yielded equations that predicted a widespread occurrence of very low FW, including those areas where  $FW_{obs}$  is very high either seasonally or throughout the year. Similarly, poor predictive models were obtained whether derived for all sites or just those restricted to specific plant functional types. These outcomes likely occur because linear regression optimises a function by minimising the error between predicted and observed values. As most grid cells have  $FW \approx 0$  (Figure 1) the ‘best’ regression equation is one that predicts FW very low almost everywhere, since in the majority of cases this is quite accurate. Efforts were made to use other optimisation criteria with customised functions that attempted to put more weight on predicting high FW correctly at the expense of larger errors where FW is low. However, these simply over predicted FW. Therefore, we were unable to find any satisfactory solution based on linear regression.

183

## 2.4 FW predicted by a nearest neighbour search

The reference data set of FW and environmental variables sites on a  $0.5^\circ$  grid at a monthly time step can be viewed as a set of data points yielding FW at many different locations in a multi-dimensional space. The eight dimensions of that space are the two climate and six vegetation variables; temperature, precipitation, leaf area index, net primary productivity, transpiration, evapotranspiration, soil water content and surface runoff. It is logical to assume that points close to each other in such a space probably have similar FW. Therefore, if we have the same environmental variables for a site of unknown FW, we can search the reference data set for its nearest neighbour, i.e. the point nearest to it. We then predict it would have the same FW as that for the nearest neighbour in the reference set, as illustrated schematically below.

1. The set of  $N$  environmental variables, suitably scaled,  $X_1, X_2 \dots X_N$ , defines an  $N$ -dimensional space

2. The Euclidean distance between two points,  $I$  and  $J$ , in this space is given by  $D_{IJ}$

$$D_{IJ} = \sqrt{\sum_{k=1,N} (X_k(I) - X_k(J))^2} \quad (2)$$

3. We calculate  $D_{IJ}$  for site  $I$  of unknown FW and all sites,  $J$ , in the reference data set, for each of which we know  $FW(J)$

4. We find  $J_{min}$ , the nearest neighbour, that which gives the lowest  $D_{IJ}$

5. We then predict  $FW(I) = FW(J_{min})$

6. If site  $I$  is classed as bare land by the DGVM, thereby having all vegetation variables = 0, we predict  $FW(I) = 0$

This nearest neighbour (NN) method can, if necessary, be extended to a KNN method, whereby rather than predicting FW based solely on the single nearest neighbour we instead consider some function of the  $K$  nearest neighbours.

208



## 209 2.5 Calculating wetland methane emissions

210 The aim of this study was to derive an algorithm for predicting wetland fraction that can then  
211 be used to calculate methane emissions. For the latter, we use the empirical method described  
212 by Cao et al. (1996), where methane production,  $mp$ , and methane oxidation,  $mo$ , rates for a  
213 specific grid cell and month are given by:

$$214 \quad mp = R_h f_t \quad (3)$$

$$215 \quad mo = mp \left( 0.6 + 0.3 \frac{GPP}{GPP_{max}} \right) \quad (4)$$

216 Where  $R_h$  is soil respiration and  $GPP$  is gross primary productivity, both obtained from the  
217 respective vegetation model.  $GPP_{max}$  is the maximum value of  $GPP$  for that grid cell for any  
218 month of the year.  $f_t$  is a function that scales for temperature,  $TMP$ , in °C.

$$219 \quad f_t = \frac{\exp(0.04055 TMP)}{3.375} \quad (5)$$

220 This is capped at a maximum value of 1. In principle there would also be a scaling function  
221 for water table depth, but this is defined as 1 for inundated wetlands and we are only  
222 modelling inundated wetland fraction, as that is how the SWAMPS-GLWD FW dataset is  
223 defined.

224 Methane emission rate,  $me$ , is then the difference between methane produced and methane  
225 oxidised, scaled by the wetland fraction for that grid cell and month

$$226 \quad me = (mp - mo) FW \quad (6)$$

227

## 228 3 Results and Discussion

### 229 3.1 Modern day test data set

230 The modern-day test set explained in Sect. 2.2 was used as a first, simple, test of the nearest  
231 neighbour algorithm for predicting FW described in Sect. 2.4. Since the modern-day test set  
232 is simply the reference climate data downscaled from 0.5° to the coarser HadCM3BL-M2.2  
233 model grid of 2.5° by 3.75° (with vegetation from the DGVMs), we expect the NN algorithm  
234 to yield predicted FW reasonably consistent with a similar downscaling of the SWAMPS-  
235 GLWD observed FW. If the NN predicted FW does not achieve this, then that would indicate  
236 that the NN algorithm has failed to predict FW sufficiently accurately. Therefore this test is  
237 primarily designed to indicate that a nearest neighbour algorithm either does or does not have  
238 the potential to be applied to paleoclimates.

239 Fig. 2 shows maps of seasonal, June–July–August and December–January–February, average  
240 FW from the observed SWAMPS-GLWD data interpolated to 2.5° x 3.75° along with the  
241 predicted FW using either SDGVM or LPJ vegetation data test sets. For both vegetation  
242 models, the predicted FW maps are similar to the observed-interpolated data. Sparse patches  
243 of high FW occur in the tropics, especially the Amazon, throughout the year, and large areas  
244 of seasonal summer wetlands occur in Alaska, Canada and Siberia. The monthly variation of  
245 FW north and south of 30° N, i.e. essentially comparing boreal and tropical wetlands is  
246 shown in Figure 3. We split the global values into these two zones because there are virtually





no southern hemisphere boreal wetlands, and any division based purely on latitude is arbitrary. The nearest-neighbour algorithm generates the correct seasonal FW pattern in boreal regions and, as expected, a relatively constant monthly FW in the tropics. However, SDGVM consistently underestimates the amount of tropical wetland, whilst LPJ agrees reasonably well with observations; mean monthly values are  $2.11$ ,  $1.47$  and  $1.90 \times 10^6 \text{ km}^2$  for the observed, SDGVM and LPJ respectively. This is due to the fact that SDGVM classes some grid cells as bare land, assumed to have  $\text{FW} = 0$  in our algorithm, even though some of these have non-zero FW in the SWAMPS-GLWD database. LPJ does not classify these grid cells as bare land but instead treats them as very low amounts of vegetation, therefore yielding higher global FW that is more consistent with observations. If we exclude from the observed data those grid cells SDGVM predicts as bare land, then the SDGVM prediction matches better the observed data and LPJ predictions (Table 1). These results give confidence that a nearest neighbour algorithm is able to reproduce acceptable FW based on these specific climate and vegetation variables.

Figure 4 shows the monthly variation in wetland methane emissions for boreal and tropical areas, calculated using: the observed or predicted FW, both vegetation models' outputs and Eq. 3 to 6. The annual methane emissions totals are summarised in Table 2, along with other recent estimates from model intercomparisons. The annual and monthly zonal methane emissions are broadly similar for a given vegetation model regardless of whether the observed or predicted FW is used. SDGVM gives global emissions in line with the other modelling studies, whereas those from LPJ are somewhat lower. This is mainly due to differences in tropical emissions. SDGVM yields higher tropical emissions than LPJ but slightly lower emissions north of  $30^\circ\text{N}$ . The main factors influencing the modelled methane emissions (other than FW) are, according to equations (3) to (5), temperature (which is the same for both vegetation models), soil respiration ( $R_h$ ) and gross primary productivity ( $GPP$ ), the latter two differing between the two vegetation models. It appears that differences in  $R_h$  lead to the different zonal methane totals. South of  $30^\circ\text{N}$  SDGVM and LPJ model annual total  $R_h$  of  $46,000 \text{ Tg C year}^{-1}$  and  $35,000 \text{ Tg C year}^{-1}$  respectively and, using the same observed FW, SDGVM and LPJ model annual methane emissions of  $123 \text{ Tg CH}_4 \text{ year}^{-1}$  and  $69 \text{ Tg CH}_4 \text{ year}^{-1}$  respectively. Therefore, in the tropics the differences in the predicted methane emissions seem to be due to differences in calculated  $R_h$ . North of  $30^\circ\text{N}$  both DGVMs have similar  $R_h$ ,  $20,000 \text{ Tg C year}^{-1}$  and  $22,000 \text{ Tg C year}^{-1}$  respectively for SDGVM and LPJ, and similar values of methane emissions,  $64 \text{ Tg CH}_4 \text{ year}^{-1}$  and  $65 \text{ Tg CH}_4 \text{ year}^{-1}$  respectively.

### 3.2 Early Eocene climate

In the previous section we have shown that a NN method can reproduce FW for a modern day climate, justifying its application to the early Eocene climate described in section 2.2. However, as noted at the end of section 2.4 a NN method can be extended to KNN, whereby we predict FW based on some function of the FW of  $K$  nearest neighbours (noting that in 3.1, NN is simply 1NN, i.e. KNN with  $K=1$ ). A 1NN algorithm that works well to predict modern day FW may not work as well for a paleo climate of many millions of years in the past. The reference data set we use, section 2.1, is very similar to the modern day test set, the latter's climate data is simply obtained by interpolating the former to a coarser spatial grid. Therefore, we expected and observed high correlation between modern day FW predicted from the nearest neighbour in the reference data and the actual FW. The early Eocene test



data has significant differences to the reference data since the climate of the early Eocene is obviously not the same as the modern day. Therefore, it will be harder for a nearest neighbour based method, searching a space described by climate and vegetation data, to find a nearest neighbour in the modern day reference data with the correct early Eocene FW, whatever that may be. It may be that for a high FW early Eocene grid cell the nearest neighbour happens to have quite low FW and vice versa. Figure.1 shows that FW can change from very high to almost zero over relatively small distances, for example in the Amazon basin, and that therefore sites with similar climate and vegetation can have very different FW. The greater the degree of difference between the early Eocene and the modern day reference data sets, the more likely it is that the first nearest neighbour does not have the correct FW.

FW calculated for the Early Eocene using the exact same INN method as used for the modern day test set yields values of global monthly mean wetland area of  $4.07 \times 10^6 \text{ km}^2$  using SDGVM. This is around 33% higher than that for the modern day,  $3.00 \times 10^6 \text{ km}^2$  from Table 1. However, this includes a contribution of  $1.53 \times 10^6 \text{ km}^2$  from areas south of  $30^\circ \text{ S}$ , which have an almost negligible contribution for the modern day, so the tropics and northern Boreal regions actually have lower FW for the Early Eocene. Given that the Early Eocene was significantly warmer and wetter than the modern day (Carmichael et. al. 2017), we expect greater wetland area than the modern day. Beerling et al. (2011) reported global wetland area for an Early Eocene climate using SDGVM; employing their method to our Early Eocene climate, so as to eliminate differences arising from the specific HadCM3 model climate and spatial resolution, yields global monthly mean FW area of  $16.29 \times 10^6 \text{ km}^2$ , four times higher than the value we would calculate from a INN method. Therefore, based on comparison with both the modern day and a previous Eocene study, it appears that a INN method may be unsuitable for a paleoclimate that is very different to our modern day reference climate, and we consider KNN with higher values of K.

### 3.2.1 maxKNN FW prediction

If indeed the INN results are too low then that implies that for some hypothetical high FW sites from the Early Eocene, the first nearest neighbours in the reference data have very low FW. Therefore, if we consider higher values of K we may improve our estimate by predicting FW to be the maximum FW of K nearest neighbours in the reference data. However, applying this approach will yield increasingly higher FW as K increases, requiring a data-constrained optimisation of K. Here we use the distribution of coal deposits in the Eocene, (Boucot et al., 2013) shown in Figure 5 as such constraints. There are some limitations to this approach. Coal is formed in wetlands, but can also form in other settings such as lakes; and of course, these datasets do not document where wetlands were present but the sedimentary record is missing or has not been published. In the tropics, coal may not have formed in wetland environments due to a very high rate of carbon cycling and in northern latitudes subsequent glaciations could have eroded coal deposits away. Moreover, data will be sparse or non-existent for remote or inaccessible modern day regions, such as under the Antarctic ice sheet. We also note that precise age and location, especially when comparing to low resolution climate simulations, could cause disagreement for grid-by-grid comparisons. A final and critical complication is that FW is a number between 0 and 1, corresponding to the fraction of a site that is wetland, whereas the coal data is a binary measure: either a grid cell





has or does not have a coal deposit within it. For all of these reasons, data-model comparisons must be done cautiously; nonetheless, these data are useful for identifying the most effective K value for reconstructing likely wetlands.

We defined two functions to assess how well a model FW matched the locations of Eocene coal deposits. Firstly,  $f1$  is defined as the mean distance, in km, of a coal deposit location to a grid cell with model FW predicted to be  $> 0.2$ . The choice of 0.2 representing significant FW is arbitrary but the analysis was repeated with other values and the same conclusions were found. Secondly,  $f2$  is defined as the mean FW of the grid cell closest to each coal deposit location, providing that site is within 2 grid points of that coal deposit location, to allow some leeway with regard to different projected locations of land masses in the early Eocene. Again the choice of a 2-pixel limit is arbitrary but the analysis was repeated with other limits and the same conclusions found.

Figure 6 shows the values of  $f1$  and  $f2$  for maxKNN predictions of FW with increasing K for both the SDGVM and LPJ Early Eocene data sets, compared to a data set of coal deposit locations. As explained, since FW increases with K then by extension, so does the likelihood of a site with a coal deposit in or close to it coinciding with a site of significant FW.

Therefore, we do not seek to find the value of K that will give the lowest value of  $f1$  and highest value of  $f2$  as that would simply be K equal to the size of the entire reference data set. Instead, we try to find the lowest value of K that gives a “good” prediction for both  $f1$  and  $f2$ . Although “good” is a subjective measure, we define it based on where increases in K result in marginal improvements in  $f1$  and  $f2$ . For both vegetation models as K increases from 1 to 3  $f1$  decreases significantly and  $f2$  increases significantly. For  $K > 3$  the decrease in  $f1$  levels out and the increase in  $f2$  also declines. Therefore, we conclude that based on comparison of predicted FW and locations of coal deposits,  $K=3$  is a reasonable choice to make predictions for our early Eocene climate via a maxKNN algorithm.

361

### 3.2.2 FW predicted by max3NN

Figure 7 shows annual maximum FW (i.e. for each pixel the highest of the 12 monthly values) calculated by a max3NN model using SDGVM or LPJ vegetation data, as described above, with the locations of early Eocene coal deposits also shown. The annual maximum FW is shown here as FW might only need to be high at some point during the year to give rise to coal deposits. The areas of predicted high FW are much larger than for the modern day (Fig. 1); moreover, at this spatial resolution there are often abrupt changes from low-medium (yellow) to much higher (red) values leading to some isolated patches of high FW. The approach makes it difficult to interrogate specific factors that drive the increase in Eocene FW compared to today but given the wetter climate of the Early Eocene higher FW than the modern day is to be expected. The patchiness is partly a consequence of using annual maximum FW but also reflects the challenge of predicting a characteristic of a paleoenvironment based on modern day reference data. Considering zonal total FW and seasonal average FW maps, i.e. averaging out some of the small scale spatial and temporal variability, is likely a better approach for understanding ancient methane cycling and these are discussed later.



378 The maps of predicted FW are quite different for the two vegetation models, but the greatest  
379 differences are in areas with very little or no coal deposits, e.g. the tropics, north eastern  
380 North America and Antarctica, making it difficult to critically evaluate them against the data.  
381 However, the monthly variations given by the two vegetation models in total FW (Figure 8)  
382 and methane emissions (Figure 9), for the three latitudinal zones are reasonably similar with  
383 respect to seasonal variations, in that both have their highest values in the summer months for  
384 zones north of 30° N and south of 30° S and no clear seasonal variation in the tropics. In the  
385 tropical zone, predictions of monthly FW area are similar in magnitude for the two vegetation  
386 models, with SDGVM usually predicting higher FW than LPJ. However, in the zone north of  
387 30° N LPJ predicts much higher FW than SDGVM throughout June to October with a peak in  
388 September, whereas SDGVM peaks in May. A similar but less striking pattern occurs for the  
389 zone south of 30°S where again LPJ predicts higher summer FW area than SDGVM. These  
390 differences between the two vegetation models are also evident in maps of seasonal average  
391 predicted FW (Figure 10). In June to August, SDGVM predicts very little wetland area in the  
392 northern hemisphere, whereas LPJ predicts moderate to high FW areas over much of the land  
393 north of around 50° N. In December to February both models predict almost zero FW north  
394 of around 50° N. In the tropics and the southern hemisphere, the two models predict similar  
395 amounts of wetland area, but with SDGVM predicting slightly higher FW overall between  
396 30° S to 30° N and LPJ predicting slightly higher FW south of 30° N.

397 This differs from the modern day distribution of wetlands (Figure 1) and likely arises from a  
398 variety of method-dependent factors. First, the coarser resolution leads to more patchy  
399 distribution, as is evident in the modern day data in Figures 1 and 2 (top row) at 0.5° x 0.5°  
400 and 2.5° x 3.75° spatial resolution. This is particularly true for the tropics where wetlands do  
401 occur in small areas. Secondly, the nature of the nearest neighbour algorithm relies on the  
402 principle that a grid cell in a paleoclimate with specific values of environmental variables will  
403 have the same FW as a grid cell in a modern day reference data set with similar values for  
404 those environmental variables; however, other factors influence wetland fraction, such as the  
405 topography. Therefore, a nearest neighbour method predicting FW for a paleoclimate from a  
406 modern day reference data may well have errors for a given grid cell and month. These errors  
407 should reduce when averaged over latitudinal zones or seasonal averages.

408 The differences between methane emissions from the two vegetation models likely arise from  
409 their respective impacts of soil water balance, via the magnitude of evapotranspiration (EVT)  
410 relative to precipitation (PRC). As the vegetation and climate models are not dynamically  
411 coupled, PRC will be the same in all Eocene simulations, but EVT will vary; thus, vegetation  
412 models that yield elevated EVT in a given grid cell are more likely to yield negative water  
413 balance (PRC-EVT) and low FW. Figure 11 shows the June to August mean PRC-EVT for  
414 SDGVM and LPJ, revealing that it is negative in most places north of 30° N for SDGVM but  
415 is slightly positive or at least much closer to zero for LPJ. Therefore, SDVGM will generally  
416 predict lower FW by identifying modern day nearest neighbours where PRC < EVT and  
417 unlikely to be wetland. The lack of extensive coal deposits in the high northern latitudes,  
418 especially where the LPJ-based approach predicts wetlands, could indicate that the LPJ  
419 approach has over-predicted FW. However, we caution that this could be a data limitation  
420 issue and future work is required to interrogate the forecasts of these two methods.  
421 Regardless, both models yield broadly similar results on global and zonal terms (Table 3)  
422 indicating that the KNN algorithm could be a useful complementary approach for



interrogating ancient wetland extent and methane emissions. Global monthly mean FW is  $8.5 \times 10^6 \text{ km}^2$  and  $10.3 \times 10^6 \text{ km}^2$  predicted by SDGVM and LPJ respectively. Both of these values are larger than for the modern day value of  $3.0 \times 10^6 \text{ km}^2$ , as we would have expected.

#### 4. Conclusions

We have presented a nearest neighbour method by which FW can be calculated at sites on the Earth's surface for an Eocene paleoclimate based on a set of environmental variables obtained from climate and vegetation models and comparison of these to a modern day reference data set. The precise formulation of the nearest neighbour approach was determined through comparison to locations of Eocene coal deposits and indicated that a max3NN method was best suited in this case. That should not be taken to imply that a max3NN would be the best in general; for another paleoclimate a similar analysis to that performed here would be required to determine the optimum implementation of KNN. The predicted distributions of FW are much higher than those of today, as we would expect. We have assessed this using two different global vegetation models, and whilst these do yield some geographical differences in FW arising from different evapotranspiration estimates, they are broadly similar when considering zonal means. For both vegetation models, global monthly mean modelled FW area is less than, around half to two thirds, that of Beerling et al., 2011, as are the values of the wetland methane emissions. However, our new method does not rely on the standard deviation of orography, a variable which is only known to a relatively coarse resolution for deep paleoclimates.

#### Code and Data

This study presents a methodology using existing data and climate and vegetation models. Information relating to these is already included in this article. Code implementing the maxKNN prediction of FW is included as supplement.

#### Author Contribution

DJW and DJB planned the work with advice from all co-authors. DJW carried out most of the experimental work with MB providing the HadCM3BL-M2.2 and EPK the LPJ model data. DJW prepared the manuscript with contributions from all co-authors.

#### Competing Interests

The authors declare that they have no conflict of interest.

#### Acknowledgements

Funding was provided by the Natural Environmental Research Council (NERC) grant NE/J00748X/1. The authors would like to thank Chris Scotese for access to and advice on Eocene coal deposit data.



## References

- Anagnostou, E., John, E. H., Edgar, K. M., Foster, G. L., Ridgwell, A., Inglis, G. N., Pancost, R. D., Lunt, D. J. and Pearson, P. N.: Changing atmospheric CO<sub>2</sub> concentration was the primary driver of early Cenozoic climate, *Nature*, 533(7603), 380–384, doi:10.1038/nature17423, 2016.
- Beerling, D. J., and Woodward, F. I.: *Vegetation and the Terrestrial Carbon Cycle: Modelling the First 400 Million Years*. Cambridge University Press, Cambridge, 2001
- Beerling, D., Berner, R. A., Mackenzie, F. T., Harfoot, M. B., and Pyle, J. A.: Methane and the CH<sub>4</sub>-related greenhouse effect over the past 400 million years, *Am. J. Sci.*, 309, 97–113, DOI 10.2475/02.2009.01, 2009.
- Beerling, D. J., Fox, A., Stevenson, D. S., and Valdes, P. J.: Enhanced chemistry-climate feedbacks in past greenhouse worlds, *Proc. Natl. Acad. Sci.*, 108, 9770–9775, doi:10.1073/pnas.1102409108, 2011.
- Beven, K.J. and Kirkby, M.J.: A physically based variable contributing area model of basin hydrology, *Hydrol. Sci. Bull.*, 24, 43–69, doi:10.1080/02626667909491834, 1979
- Boucot, A.J., Chen X., and Scotese, C.R.: *Phanerozoic Paleoclimate: An Atlas of Lithologic Indicators of Climate*, *SEPM Concepts in Sedimentology and Paleontology*, (Digital Version), No. 11, ISBN 978-1-56576-281-7, Society for Sedimentary Geology, Tulsa, OK, 478 pp., 2013.
- Cao, M., Marshal S., and Gregson, K.: Global carbon exchange and methane emissions from natural wetlands: Application of a process-based model, *Journal of Geophysical Research*, 101, 14399–14414, doi.org/10.1029/96JD00219, 1996
- Carmicheal, M.J., Gordon, N.I., Badger, M.P.S, Naafs, B.D.A., Behrooz, L., Rimmelzwaal, S., Monteiro, F.M., Rohrsen, M., Farnsworth, A., Buss, H.L., Dickson, A.J., Valdes, P.J., Lunt, D.J., and Pancost, R.D.: Hydrological and associated biogeochemical consequences of rapid global warming during the Paleocene-Eocene Thermal Maximum, *Global and Planetary Change*, 157, 114–138, doi:10.1016/j.gloplacha.2017.07.014, 2017.
- Global Land Cover 2000 database. European Commission, Joint Research Centre, <http://forobs.jrc.ec.europa.eu/products/glc2000/glc2000.php>, 2003, accessed 2005.
- IPCC, 2013: *Climate Change 2013: The Physical Science Basis. Contribution of Working Group I to the Fifth Assessment Report of the Intergovernmental Panel on Climate Change* [Stocker, T.F., D. Qin, G.-K. Plattner, M. Tignor, S.K. Allen, J. Boschung, A. Nauels, Y. Xia, V. Bex and P.M. Midgley (eds.)]. Cambridge University Press, Cambridge, United Kingdom and New York, NY, USA, 1535 pp.
- Lehner, B. and Doll, P.: Development and validation of a global database of lakes, reservoirs and wetlands, *Journal of Hydrology*, 296, 1–22, doi:10.1016/j.jhydrol.2004.03.028, 2004
- Lu, X. and Zhuang, Q.: Modeling methane emissions from the Alaskan Yukon River basin, 1986–2005, by coupling a large-scale hydrological model and a process-based methane model, *J. Geophys. Res.*, 117, G02010, doi:10.1029/2011JG001843, 2012.



- 506  
507  
508 Melton, J. R., Wania, R., Hodson, E. L., Poulter, B., Ringeval, B., Spahni, R., Bohn, T., Avis,  
509 C. A., Beerling, D. J., Chen, G., Eliseev, A. V., Denisov, S. N., Hopcroft, P. O., Lettenmaier,  
510 D. P., Riley, W. J., Singarayer, J. S., Subin, Z. M., Tian, H., Zürcher, S., Brovkin, V., van  
511 Bodegom, P. M., Kleinen, T., Yu, Z. C., and Kaplan, J. O.: Present state of global wetland  
512 extent and wetland methane modelling: conclusions from a model inter- comparison project  
513 (WETCHIMP), *Biogeosciences*, 10, 753–788, doi:10.5194/bg-10-753-2013, 2013.
- 514 Papa, F., C. Prigent, F. Aires, C. Jimenez, W. B. Rossow, and E. Matthews. Interannual  
515 variability of surface water extent at the global scale, 1993–2004, *J. Geophys. Res.*, 115,  
516 D12111, doi:10.1029/2009JD012674, 2010
- 517 Poulter, B., Bousquet, P., Canadell, J. G., Cias, P., Peregon, A., Saunio, M., Vivek, K. A.,  
518 Beerling, D., Brovkin, V., Jones, C. D., Joos, F., Gedney, N., Ito, A., Kleinen, T., Koven, C.,  
519 McDonald, K., Melton, J. R., Peng, C., Peng, S., Prigent, C., Schroder, R., Riley, W., Saito,  
520 M., Spahni, R., Tian, H., Taylor, L., Viovy, N., Wilton, D., Wiltshire, A., Xu, X., Zhang, B.,  
521 Zhang, Z., and Zhu, Q.: Global wetland contribution to 2000–2012 atmospheric methane  
522 growth rate dynamics, *Environ. Res. Lett.*, 12, 094013, doi:10.1088/1748-9326/aa8391, 2017
- 523 Prigent, C., F. Papa, F. Aires, W. B. Rossow, and E. Matthews. Global inundation dynamics  
524 inferred from multiple satellite observations, 1993–2000. *J. Geophys. Res.*, 112, D12107,  
525 doi:10.1029/2006JD007847, 2007.
- 526  
527 Schroeder, R., McDonald, K. C., Chapman, B. D., Jensen K., Podest, E., Tessler Z. D., Bohn,  
528 T. J., and Zimmermann, R.: Development and Evaluation of a Multi-Year Fractional Surface  
529 Water Data Set Derived from Active/Passive Microwave Remote Sensing Data, *Remote*  
530 *Sensing*, 7, 16688–16732, doi:10.3390/rs71215843, 2015.
- 531 Sloan, L. C., Walker, J. C. G., Moore Jr, T. C., Rea, D. K., and Zachos, J. C.: Possible  
532 methane-induced polar warming in the early Eocene, *Nature*, 357, 320–322,  
533 doi:10.1038/357320a0 1992.
- 534 Stocker, B. D., Spahni, R. and Joos, F.: DYTOP: a cost efficient TOPMODEL  
535 implementation to simulate sub-grid spatio-temporal dynamics of global wetlands and  
536 peatlands, *Geosci. Model Dev.*, 7, 3089–3110, doi:10.5194/gmd-7-3089-2014, 2014.  
537
- 538 Valdes P. J., Beerling D. J. and Johnson, C. E.: The ice age methane budget, *Geophys. Res.*  
539 *Lett.*, 32, L02704, doi:10.1029/2004GL021004, 2005.
- 540  
541 Valdes, P. J., Armstrong, E., Badger, M. P. S., Bradshaw, C. D., Bragg, F., Davies-Barnard,  
542 T., Day, J. J., Farnsworth, A., Hopcroft, P. O., Kennedy, A. T., Lord, A. S., Lunt, D. J.,  
543 Marzocchi, A., Parry, L. M., Roberts, W. H. G., Stone, E. J., Tourte, G. J. L., and Williams, J.  
544 H. T.: The BRIDGE HadCM3 family of climate models: HadCM3@Bristol v1.0, *Geosci.*  
545 *Model Dev.*, 10, 3715–3743, doi:10.5194/gmd-10-3715-2017, 2017
- 546  
547 Wania, R., Ross, I., and Prentice, I. C.: Integrating peatlands and permafrost into a dynamic  
548 global vegetation model: 1. Evaluation and sensitivity of physical land surface processes,  
549 *Global Biogeochem. Cycles*, 23, GB3014, doi:10.1029/2008GB003412, 2009.



550  
551 Wei, Y., Liu, S., Huntzinger, D. N., Michalak, A. M., Viovy, N., Post, W. M., Schwalm, C.  
552 R., Schaefer, K., Jacobson, A. R., Lu, C., Tian, H., Ricciuto, D. M., Cook, R. B., Mao, J., and  
553 Shi, X.: The North American Carbon Program Multi-scale Synthesis and Terrestrial Model  
554 Intercomparison Project - Part 2: Environmental driver data, Geoscientific Model  
555 Development, 7(6), 2875-2893, doi:10.5194/gmd-6-2121-2013, 2014  
556  
557 Westermann, P.: Temperature regulation of methanogenesis in wetlands, Chemosphere, 26,  
558 321-328, doi:10.1016/0045-6535(93)90428-8, 1993.  
559  
560 Whiticar, M. J.: Carbon and hydrogen isotope systematics of bacterial formation and  
561 oxidation of methane, Chem. Geol., 161, 291-314, doi:10.1016/S0009-2541(99)00092-3,  
562 1999.  
563  
564 Woodward, F., Smith, T. and Emanuel, W.: A global land primary productivity and  
565 phytogeography model, Glob. Biogeochem. Cycles, 9, 471-490, 1995  
566  
567 Zachos, J. C., Dickens, G. R., and Zeebe, R. E.: An early Cenozoic perspective on  
568 greenhouse warming and carbon-cycle dynamics, Nature, 451, 279-283,  
569 doi:10.1038/nature06588, 2008.  
570



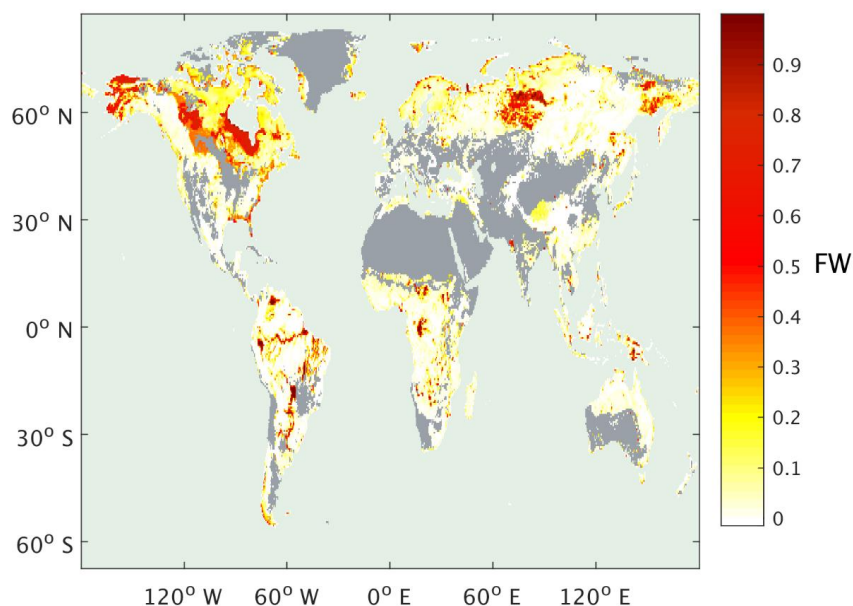


**Figure 1: Annual maximum observed FW from the SWAMPS-GLWD data set (Poulter et. al., 2017), mean of 2000 to 2012. Grey shading indicates bare land, as predicted by SDGVM, or > 50% cultivated (Global Land Cover 2000 database, 2003).**

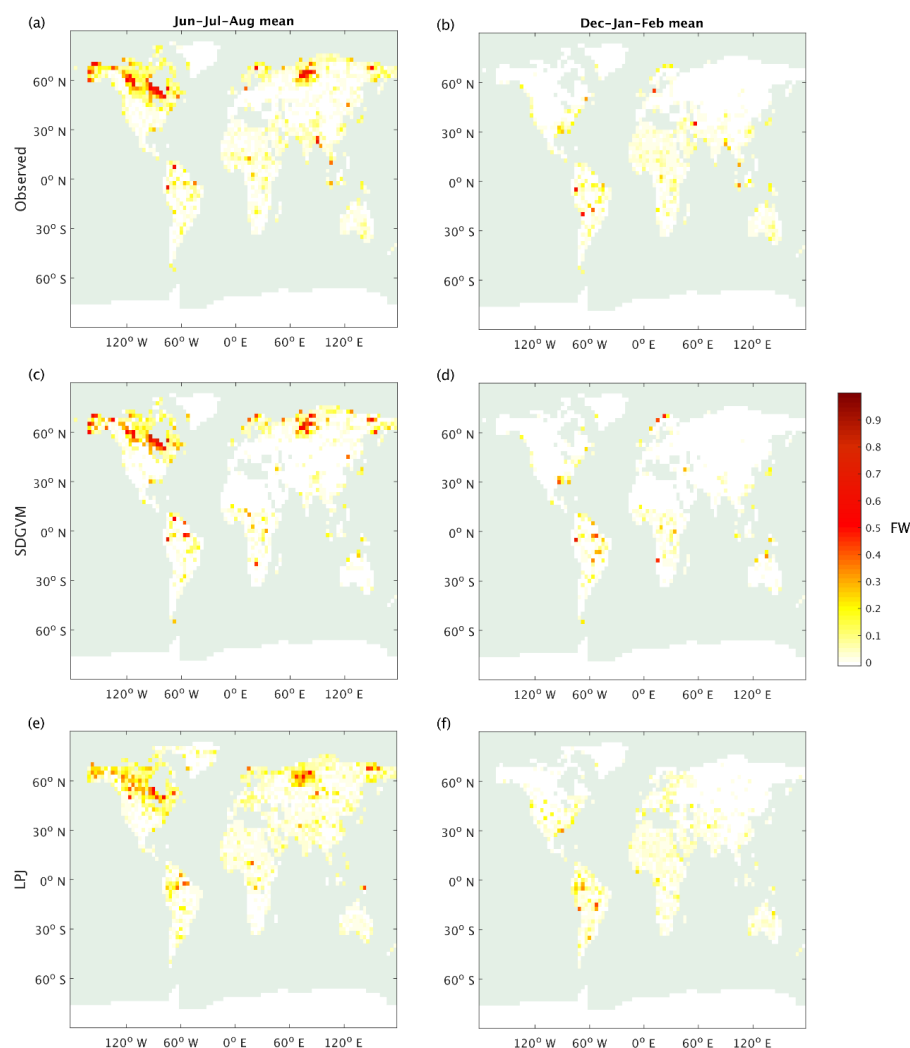


**Figure 2: Seasonal mean FW. Observed interpolated to model grid; (a) Jun–Jul–Aug and (b) Dec–Jan–Feb. 1NN prediction by SDGVM (c) Jun–Jul–Aug and (d) Dec–Jan–Feb. 1NN prediction by LPJ (e) Jun–Jul–Aug and (f) Dec–Jan–Feb.**

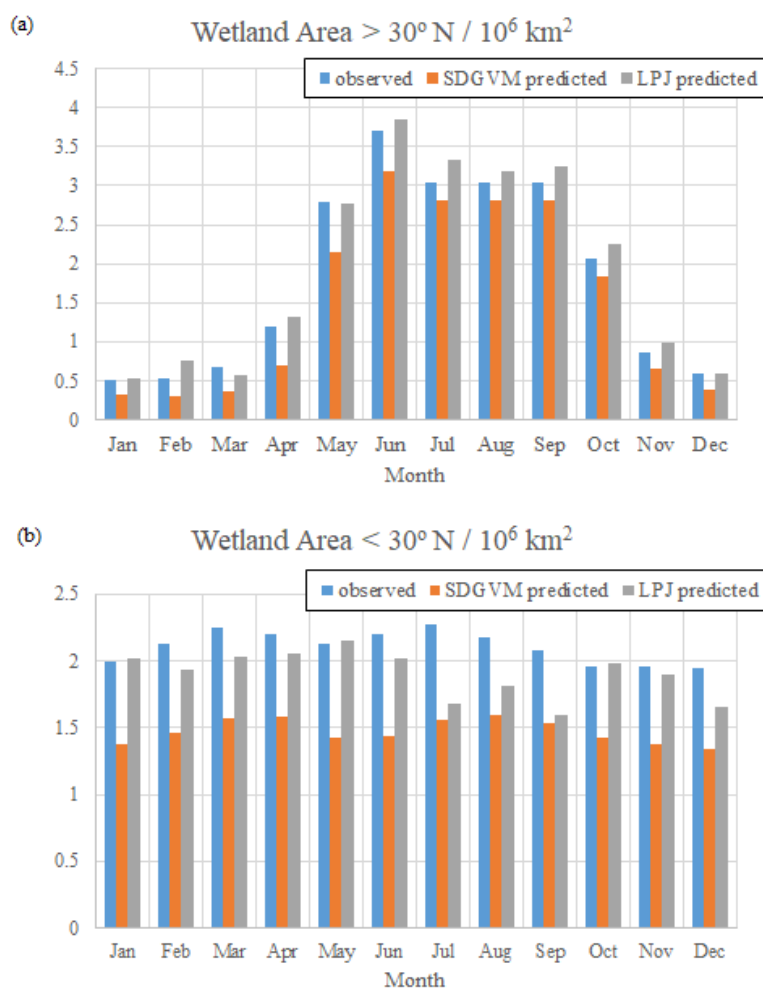


**Figure 3: Monthly zonal variations of FW calculated for the mean 2000-12 climate on a 2.5 x 3.75° grid, (a) North of 30° N and (b) South of 30° N.**

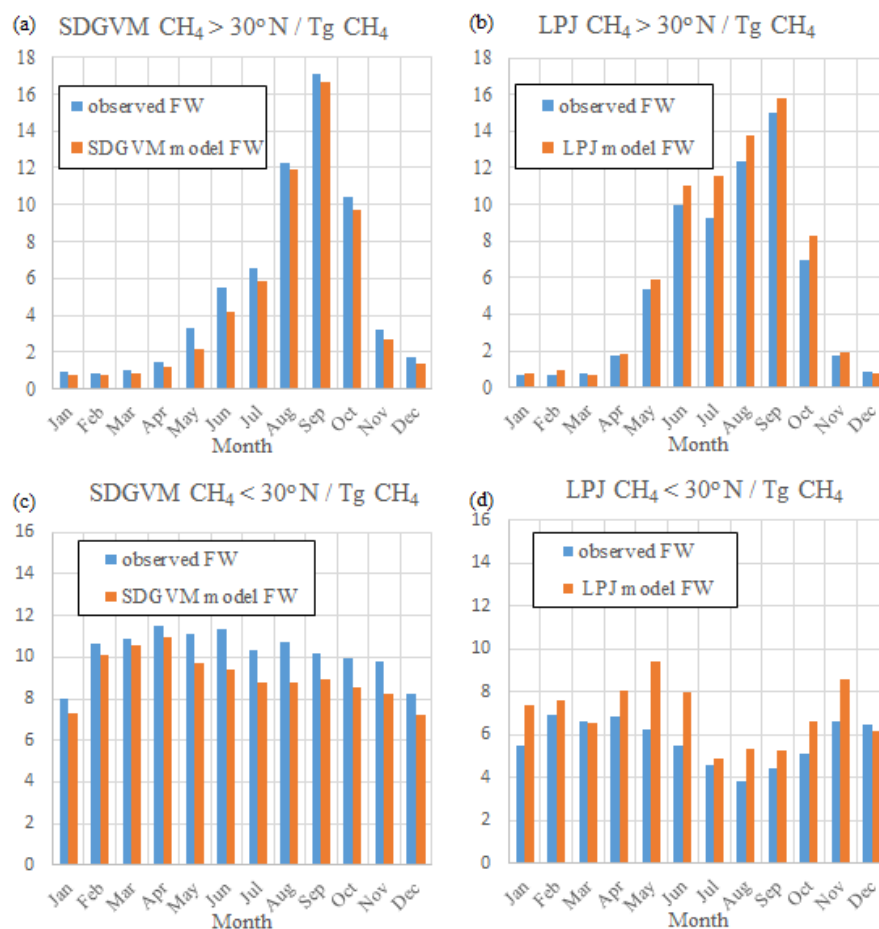
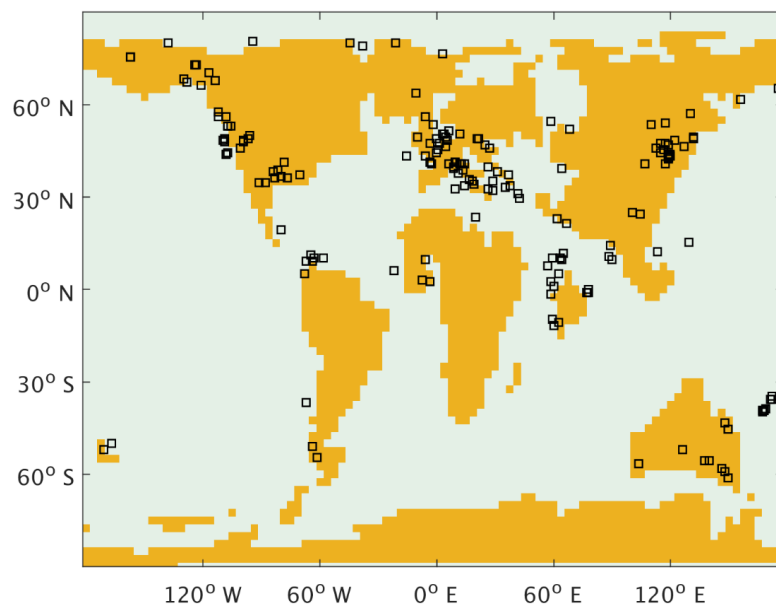


**Figure 4: Monthly zonal variations of wetland  $\text{CH}_4$  calculated from DGVM model data and observed or modelled FW, for the mean 2000-12 climate on a  $2.5 \times 3.75^\circ$  grid. (a) SDGVM North of  $30^\circ \text{N}$ , (b) LPJ north of  $30^\circ \text{N}$ , (c) SDGVM South of  $30^\circ \text{N}$  and (d) LPJ south of  $30^\circ \text{N}$ .**



591

592 **Figure 5: Locations of Eocene coal deposits plotted on our Eocene model land mask.**

593 **□ indicates an Eocene coal deposit location (Boucot et al., 2013)**

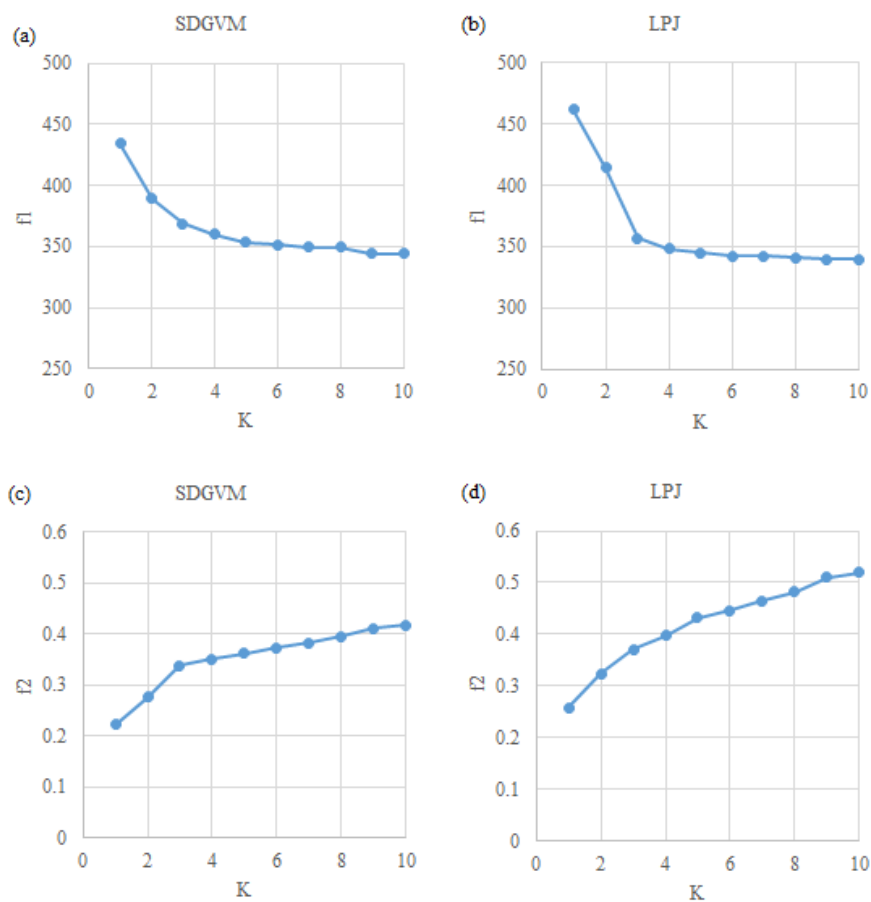


**Figure 6: Variations of statistics for match between Eocene maxKNN predicted high FW and coal locations (Boucot et al., 2013).  $f_1$  is the mean distance of a coal location to site with  $FW > 0.2$  for model based on (a) SDGVM and (b) LPJ.  $f_2$  is the mean FW of sites within 2 pixels of a coal location for model based on (c) SDGVM and (d) LPJ data.**



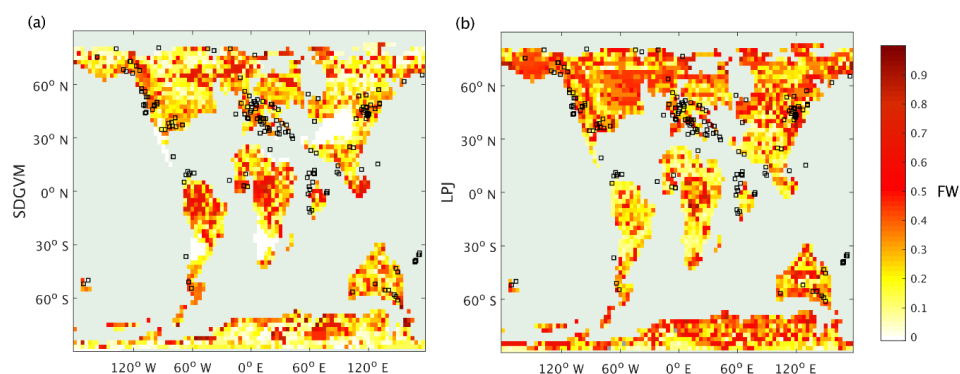


**Figure 7: Annual maximum FW calculated by the max3NN method by SDGVM and LPJ for the Eocene climate, compared with coal deposit locations**

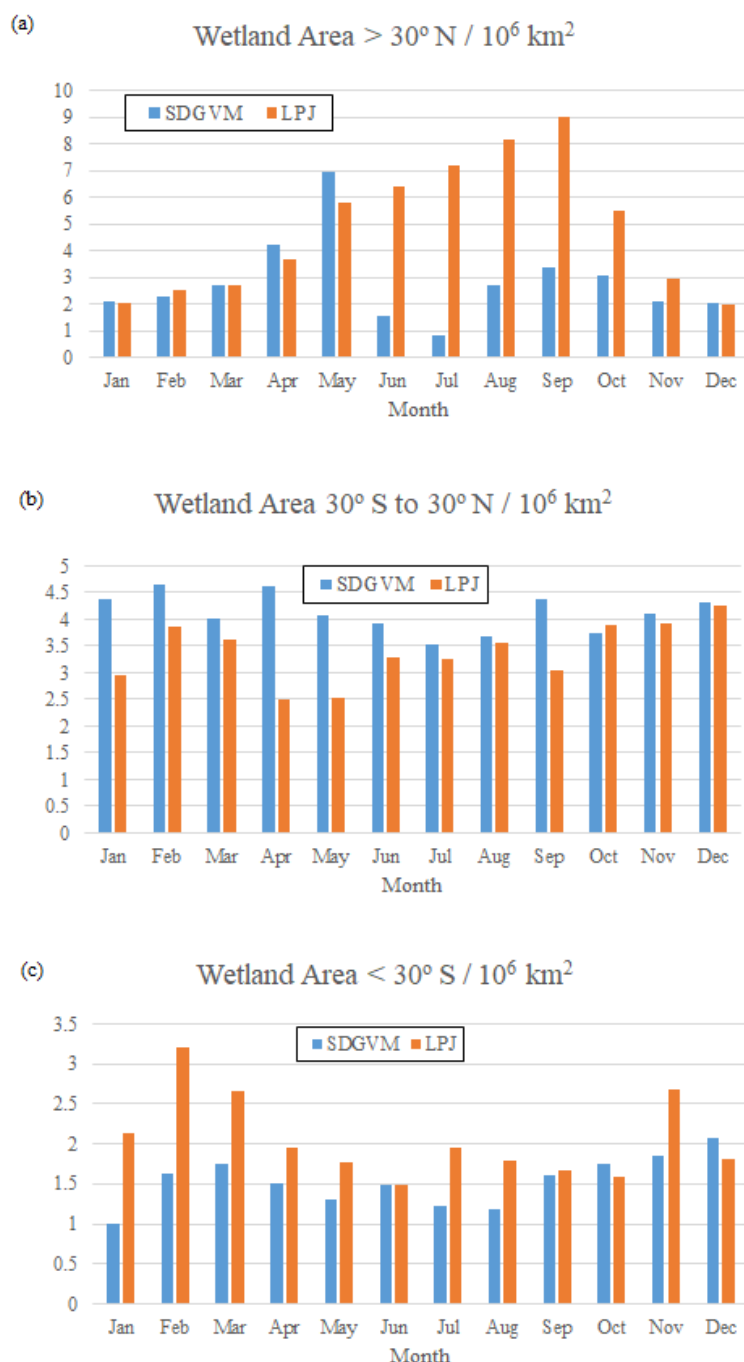
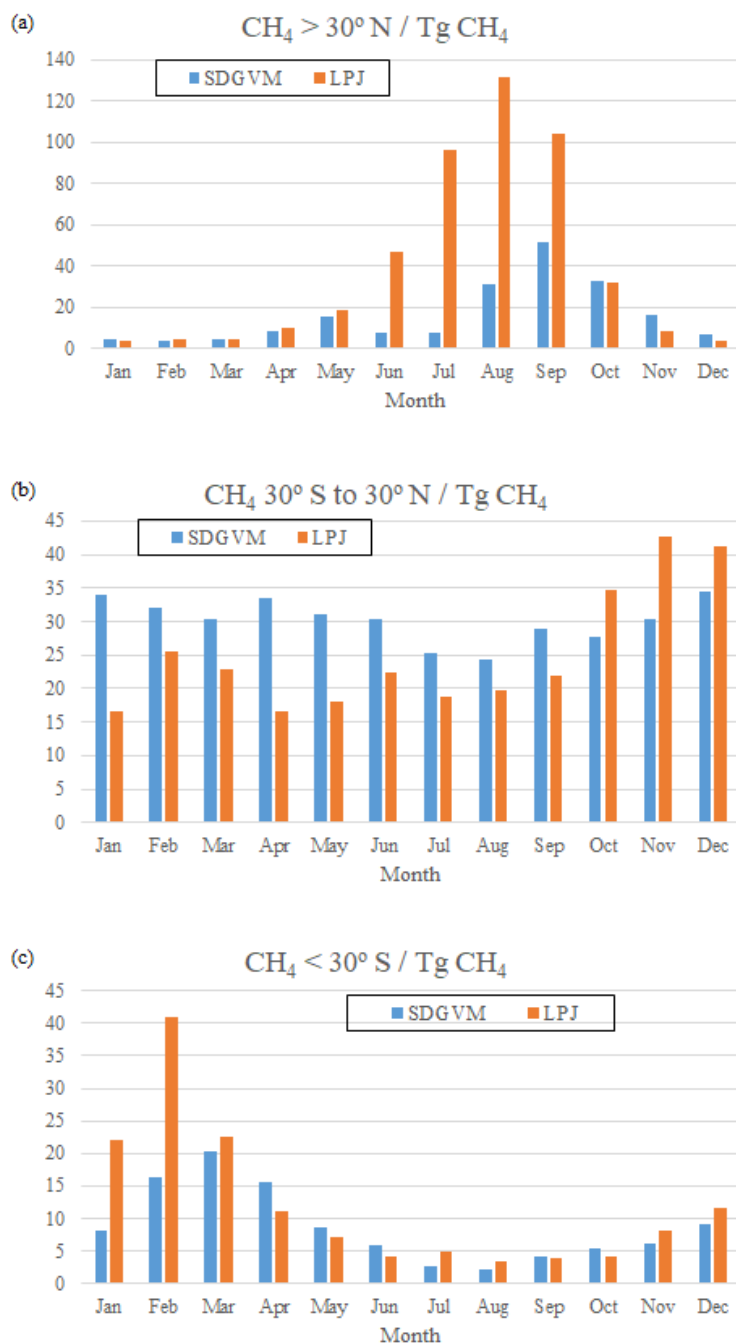


**Figure 8: Monthly variations of total wetland area calculated for the Eocene climate by SDGVM and LPJ, for (a) all areas north of 30° N, (b) all areas between 30° S and 30° N and (c) all areas south of 30° S.**



608  
 609 **Figure 9: Monthly variations of wetland  $\text{CH}_4$  calculated from predicted FW, for the**  
 610 **Eocene climate by SDGVM and LPJ, for (a) all areas north of  $30^\circ \text{N}$ , (b) all areas**  
 611 **between  $30^\circ \text{S}$  and  $30^\circ \text{N}$  and (c) all areas south of  $30^\circ \text{S}$ .**

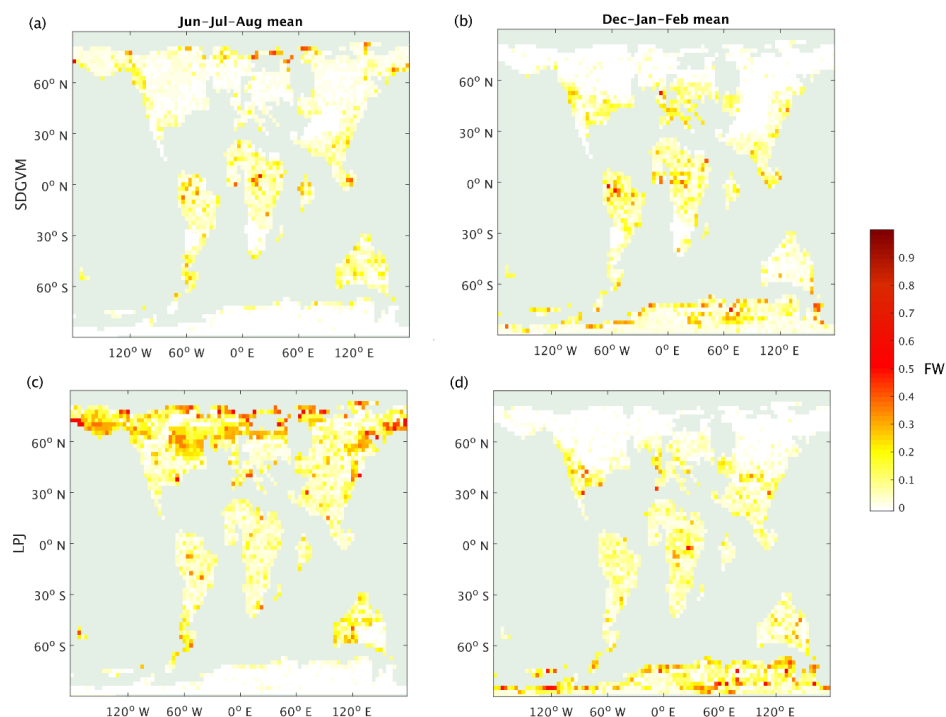


**Figure 10: Seasonal mean FW predicted for the Eocene climate by SDGVM and LPJ using the max3NN (a) SDGVM June–July–August, (b) SDGVM December–January–February, (c) LPJ June–July–August, (d) LPJ December–January–February**

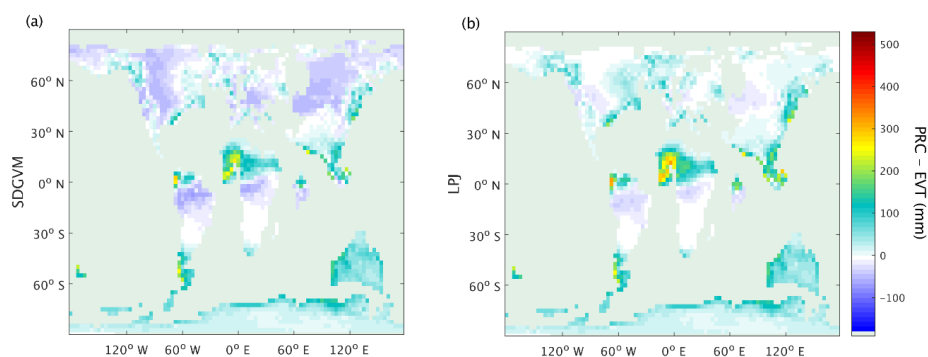


**Figure 11: June–July–August mean precipitation minus evapotranspiration for the Eocene climate, using evapotranspiration from (a) SDGVM or (b) LPJ.**



	> 30° N FW	< 30° N FW	Global FW
<b>Observed</b>	1.84	2.11	3.95
<b>Observed</b>	1.47	1.41	2.88
<b>excluding SDGVM bare land</b>			
<b>SDGVM</b>	1.53	1.47	3.00
<b>LPJ</b>	1.95	1.90	3.86

621

622

623

624

**Table 1: Modern day monthly mean FW area ( $10^6$  km<sup>2</sup>), for observed data interpolated to the 2.5° x 3.75° grid or calculated by vegetation model.**





Model	FW data	> 30° N CH <sub>4</sub>	< 30° N CH <sub>4</sub>	Global CH <sub>4</sub>
SDGVM	observed	64.32	122.69	187.01
	predicted	57.95	108.63	166.58
LPJ	observed	65.43	68.60	134.03
	predicted	73.11	83.78	156.89
GCP-CH <sub>4</sub> *	observed 0.5°			~ 184
WETCHIMP**	model specific	51±15	126±31	190±39

\* GCP-CH<sub>4</sub> (Poulter et al., 2017) results are the mean of 11 different methane emission models with the same observed wetland data as used to produce Figure 1 here. They are quoted as means over specific ranges of years; 2000–2006 = 184.0 ± 21.1, 2007–2012 = 183.5 ± 23.1, 2012 = 185.7 ± 23.2. As our results are for a single mean 2000–12 year we therefore only quote an approximate value from this source for comparison.

\*\* WETCHIMP (Melton et al., 2013) results are the mean of 8 different models, 1993–2004, each of which used their own definition of wetland extent rather than observed data

**Table 2: Modern day annual total wetland CH<sub>4</sub> emission (Tg CH<sub>4</sub> year<sup>-1</sup>), calculated by vegetation model using either observed FW data (interpolated to the 2.5° x 3.75° grid) or model predicted FW, compared with other modelling studies.**



638

<b>FW model</b>	<b>&gt; 30°N</b>	<b>30°S to 30°N</b>	<b>&lt; 30°S</b>	<b>Global</b>
<b>SDGVM</b>	2.82	4.11	1.53	8.48
<b>LPJ</b>	4.84	3.39	2.06	10.29

639 **Table 3: Eocene monthly mean max3NN modelled FW area / 10<sup>6</sup> km<sup>2</sup>**